INTERNATIONAL JOURNAL OF
COASTAL & OFFSHORE ENGINEERING IJCOE Vol.3/No. 3/Autumn 2018 (53-62)

Available online at: http://ijcoe.org/browse.php?a_code=A-10-224-1&sid=1&slc_lang=en

Wave Climate Variability and Longshore Sediment Transport Evaluation along Ramin Harbor, Southeast Coast of Iran

Ehsan Isaie Moghaddam[1*], Habib Hakimzadeh[2]

[1*] *MSc, Faculty of Civil Engineering, Sahand University of Technology; e_isaie@sut.ac.ir*
[2] *Professor, Faculty of Civil Engineering, Sahand University of Technology; hakimzadeh@sut.ac.ir*

ARTICLE INFO

Article History:
Received: 26 Apr. 2018
Accepted: 26 Nov. 2018

Keywords:
Longshore Sediment Transport
Wave Climate
Seasonal Variations
Ramin Harbor
Monsoon Season
Kamphuis Formula

ABSTRACT

This paper examines the variation of wave characteristics and net Longshore Sediment Transport (LST) rates along the Ramin Harbor, southeast coast of Iran. Potential LST rates were determined based on three empirical relationships, namely, CERC, Kamphuis and Komar and using transformed hindcast offshore waves from 1985 to 2006. Detailed analysis of 22-year deep water wave information for the region indicates considerable seasonal variations for the wave conditions, with high energy monsoon waves being generated in Indian Ocean and Arabian Sea from southern direction during monsoon season. Moreover, the long period swell waves originated from Indian Ocean usually approach the coast from southeast to south. Further, the variable sea waves characterized by shorter-period, normally spreading from west to southwest, are superimposed on the basis swell during non-monsoon season. In order to assess the reliability and accuracy of the predicted magnitudes for LST rates, the achieved results were compared with the field data, with the Kamphuis equation being found to give acceptable estimation for the potential LST rate. Finally, through morphological analyze of the adjacent shorelines and coastal region, a reasonable agreement was established for the LST direction.

1. Introduction

A proper knowledge of sediment transport processes along beaches is of significant importance for engineers in coastal planning facilities. Assessment of the sediment transport rate and its predominant direction are known as important data in designing of shore protection measures. Also, it has been known that among different coastal processes and parameters, Longshore Sediment Transport (LST) is the most important parameter that controls the sediment dynamics and diverse morphological changes (Güner, Yüksel, and Çevik, 2013). It also provides an integral part of the input required for determination of dredging requirements at a port entrance (Schoonees, 2000). Furthermore, it is generally accepted that wave action is the primary source of energy available at a coastline compared to the other oceanographic parameters such as winds, tides and ocean currents for moving sediments (Prasad and Reddy, 1988). Breaking of waves as they approach to the nearshore zone is primarily associated with large amount of wave energy losses and producing the longshore currents which transport significant amount of sediments along the coast (Kunte and Wagle, 1993).

The contribution of different terms to the magnitude of the LST rate has been investigated by a number of researchers over the last decades (e.g., Camenen and Larroudé, 2003; Chempalayil et al., 2014; King, 2005; Larangeiro and Oliveira, 2003; Shanas and Sanil Kumar, 2014; Smith, Wang, Ebersole, and Zhang, 2009). It is also possible to calculate the transport rate utilizing various formulas and methods (Mafi, Yeganeh-Bakhtiary, and Kazeminezhad, 2013). Because of the complexity of the nearshore processes, numerical schemes are known to be the best tool available to describe the mechanisms governing coastal processes. But due to the extreme difficulty of acquiring extensive data over a complicated coastal topography and relatively high cost in conjunction with measurement processes, a commonly used approach is to estimate LST rate through empirical bulk formulations. Most of the LST empirical relationships suggested by researchers were extended based on laboratory data and can only be reliable for a specific circumstance. Thus, it was known that for a proper evaluation of the LST in a coastline which is subjected to various wave conditions, examination of the underlying processes and elements responsible for the

changes would be necessary (Sheela Nair, Sundar, and Kurian, 2015).

The present paper aims to investigate the long-term wave climatology of the Ramin Harbor using 22 years hindcasted wave data provided by the Iranian Ports and Maritime Organization (PMO). Seasonal to decadal variability of the LST is estimated based on empirical formulas over the period of 1985-2006. Morphological landforms and dredging statistics are used to evaluate the reliability of potential sediment transport rate along the study area. In addition, LST direction is determined through the calculations and littoral environmental observations.

2. Study area

2.1. Geomorphology

The study area in this research is Ramin fishery harbor, located in southeast of Iran, along the north coast of Oman Sea at 60.745° E longitude and 25.268°N latitude (Figure 1). The harbor layout is such that its basin's mouth is located in front of a broken coastline and the navigations through the harbor entrance are subjected to a considerable sedimentation problem due to uncontrollable sediment drift towards the harbor entrance. Consequently, the water depth at the entrance and inside the basin decreases continuously. The harbor lies in a relatively straight coastline between Beris Headland and Chabahar Bay. This section faces the Arabian Sea and the Indian Ocean and the coastline has an extension of 60 km with more or less a WNW-ESE general orientation. The bottom contours align approximately parallel to the general trend of the shoreline. The area is mainly occupied by a series of cliffs and rocky landforms both on the eastern and western side, and short stretches of sandy beaches are located to the east of the harbor and the seasonal Lipar River at a distance of 8 km east of the harbor which is blocked by sand bar. Measurements of particle size distribution at a number of locations around the basin revealed that the bottom sediment size varies along the study area from fine sand to medium sand (with a median grain size of about 0.15 mm to 0.35 mm). Also, a bathymetric survey of the near-shore zone of the Ramin Harbor indicated that the beach and near-shore profiles are characterized by a relatively steep beach slope (The overall slope in the surf-zone was found to be in the order of about 0.05).

2.2. Winds

The Arabian Sea and the Gulf of Oman are subject to two distinct seasons separated by two short (30 to 45 days) transition periods. During December through March the winds blow predominantly from the northeast and during June through September they blow from the southwest. April and May; October and November are typically the spring and fall transition, respectively. From the standpoint of wave generation,

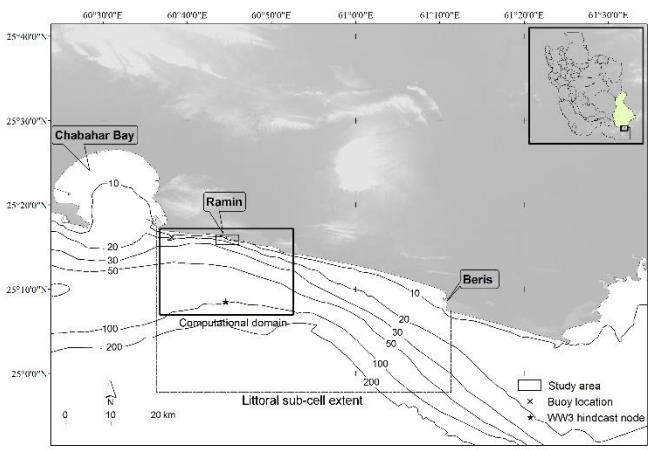

Figure 1. Location map with the position of observed and modeled waves and the extent of the regional and the nested type of unstructured grids used for nearshore wave transformation

northeast monsoon winds have no effect on the Oman Sea coast of Iran and particularly the Ramin Harbor, while southwesterly flow directly influences the study region coast (Walters and Sjoberg, 1988).

2.3. Hydrodynamics

This seasonal cycle of winds leads to a cycle in wave climate of the southeast coast of Iran, both over the open sea and over coastal areas. Hence, the study area is strongly influenced by high energy monsoon-induced waves being generated in the Indian Ocean and Arabian Sea from the southern direction during monsoon season (i.e., June to September). Furthermore, the coast is exposed to long period swell waves originating from the Indian Ocean and approaching from the sector between southeast to southern directions as well as generally the less-energetic sea waves which are propagating from west to southwest and being generated close to the shore by local Oman Sea winds, superimposed on the basis swell during non-monsoon season (i.e., October to May) (Figure 2) (Dibajnia, Kebriaee, and Allahyar, 2008).

Tides in the study area are mixed semi-diurnal dominant with a mean tidal range of 2.5 m and hence, the beach is categorized as a meso-tidal beach (Short, 1991). In meso-tidal condition, waves as well as tidal currents are important. However, in coastal regions where high energy waves are most dominant upon the shore planform, tidal influences usually become negligible (Short and Hesp, 1982). despite the low energy wave climates that exist in the study region during non-monsoon period, the high energy waves become predominant in the monsoon season.

3. Data and Methodology

Recent advancements in wave hindcast modeling provided the computation of extended, high-quality, continuous-wave time series, improving the information of the long-term wave climatology along the Iranian coasts.

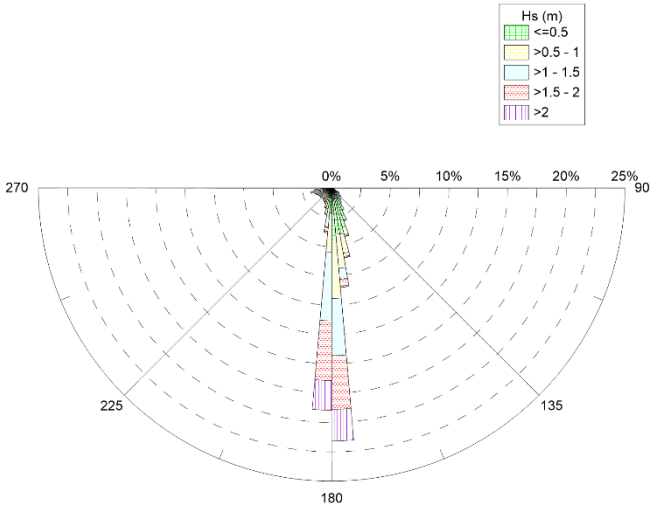

Figure 2. Long-term wave statistics of Ramin deep water location during the years between 1985 and 2006 (WW3 hindcast node)

Monitoring and Modeling Studies of Iranian Coasts is a multi-year study to determine wave climate on the Oman Sea and the Persian Gulf coastline of Iran and is based on numerical hindcast data provided by Iranian PMO. PMO hindcast wave estimates were compiled in intermediate to deep water depths with third-generation spectral wave model WAVEWATCH III (Tolman, 2009), and the achieved model results were found in excellent agreements with the measurements made at various buoy locations and satellite altimeter data (Dibajnia et al., 2008).

3.1. Wave Propagation Model Description

The wave conditions applied in the present study obtained from the aforementioned project at node 60.75° E and 25.125° N that extend from January 1985 to December 2006 with a 3-h interval. In order to assess the wave conditions in the near-shore and coastal zones which most often involves transformation of the known offshore wave statistics, MIKE 21 Spectral Wave model (MIKE 21 SW) was used. The model is based on flexible mesh and therefore particularly applicable for simultaneous wave analysis both in regional and local scales. In MIKE 21 SW model, the governing equation is based on the wave action conservation formulation given as:

$$\frac{\partial N}{\partial t} + \frac{\partial C_x N}{\partial x} + \frac{\partial C_y N}{\partial y} + \frac{\partial C_\sigma N}{\partial \sigma} + \frac{\partial C_\theta N}{\partial \theta} = \frac{S}{\sigma} \qquad (1)$$

The left-hand side of this equation describes the wave spectral energy propagation in space and time and the right-hand side term contains the superposition of source functions describing various physical phenomena. The parameters in this equation are: N = the action density spectrum, which is equal to energy density spectrum divided by the relative angular frequency, σ = wave relative angular frequency, θ = wave direction, C_x, C_y, C_σ and C_θ is the propagation velocity of a wave group in the four-dimensional phase space $\vec{x}$ (x,y), σ and θ respectively, and S = the source term for the energy balance equation. The model is used for both offshore and nearshore wave modeling as it includes two different formulations: (a) directional decoupled parametric formulation and (b) fully spectral formulation (DHI Manual, 2014). In this study, the spectral formulation and time formulation of wave model have been selected as directionally decoupled parametric formulation and quasi-stationary, respectively. The regional modeled domain extends from Ramin coast to the WW3 simulation point in the N/S direction and from east of Chabahar Bay to a midway between the Chabahar and Beris fishery port in the W/E direction. Also, the local modeled domain extends 4.2 km along the shoreline and about 2 km across the shoreline and toward the open sea where water depth is about 25 m (Figure 1). The model has been run over unstructured grids in which a coarse mesh is used for the regional scale section of the computational domain with a high-resolution mesh describing the shallow water environment at the coastline. The grids' data were achieved through interpolation of bathymetric data resulting from a compilation of the near-shore survey data with a digitized nautical hydrographic chart. Grid generation and bathymetry interpolation were accomplished by Mesh Generator, a pre-processing module of the MIKE model. The relevant size of triangle mesh varies from 1000 m to 80 m for the regional model, and varies from 100 m to 20 m for the local high-resolution model. Wave estimates derived from the WW3 hindcast of Iranian PMO at the node (60.75° E, 25.125° N; Figure 1) act as the boundary conditions along the offshore model boundary for the local wave simulation. The formulation of wave breaking derived by Battjes and Janssen (1978) is used, where α = 1 and γ = 0.85. The Nikuradse roughness coefficient is used for the dissipation due to wave-bottom friction with a physical roughness of K_N = 0.065 m.

Table 1. Statistical results of model/measure comparison at buoy location

Wave parameters	Bias	RMSE	Scatter index (%)	Correlation	Number of observation
Significant wave height (m)	0.07	0.27	33	0.87	142
Wave period (sec)	-0.11	0.57	18	0.78	
Mean wave direction (deg)	-0.59	13.06	11	N.A.	

For this particular study, since the model was only deployed for transformation of offshore wave statistics,

all wind-wave generation components (white-capping and quadruplet-wave interactions) were excluded.

In order to validate the model output parameters, a comparison is made between numerical model results against measured data at the Chabahar buoy location. The recorded data were collected at 3 h intervals using a Datawell Directional Waverider buoy near the Chabahar Bay (60.65° E and 25.267° N) from May 1998 to September 2000 discontinuously, which is deployed at 17 m water depth (Figure 1). The results, depicted in Figure 3 and Table 1, exhibit a relatively good agreement between the numerical model results and measured data. Moreover, in order to reduce running time, simulations were carried out using the annual representative wave bands for each year from 1992 to 2006 as the offshore forcing. Wave outputs were extracted along a cross-shore profile that extends from shoreline to approximately 20 m below LAT on the updrift side of the harbor (east side). Breaking wave characteristics were obtained at the point where the breaking criteria (H_s/d_b=0.78; CERC, 1984) was satisfied. These parameters were then used as the inputs for the following selected transport formulas. The instantaneous potential LST rate calculated for each wave band was converted into the annual transport considering the annual percent occurrence of each band.

3.2. Longshore Sediment Transport Formulas

Estimation of LST rates were computed using three different bulk formulations proposed by CERC (1984), Kamphuis (1991) and Komar (1998). Empirical formulas which have been used to predict potential LST rate, derived from extensive field measurements and laboratory investments and considering different parameters in formulations result in different predicts of LST value.

3.2.1. CERC formula (1984)

One of the most widely used relationships for computing LST rate is the CERC (1984) formula, which assumes proportionality between the volume of transported sediments and the longshore energy flux. The CERC formula is defined by:

$$Q = \frac{K}{(\rho_s-\rho_w)(1-n)g}\frac{\rho_w g}{16}H_{sb}{}^2 C_{gb}\sin(2\alpha_b) \qquad (2)$$

Where Q represents the LST rate in volume per unit time, K is a dimensionless empirical proportionality coefficient and was taken as 0.39, ρ_w is the density of saltwater, ρ_s is the sediment density, g is the gravity acceleration, n is the porosity of sediments, H_{sb} is the significant breaking wave height, C_{gb} is the wave group celerity at the breaker line and α_b is the wave breaking angle.

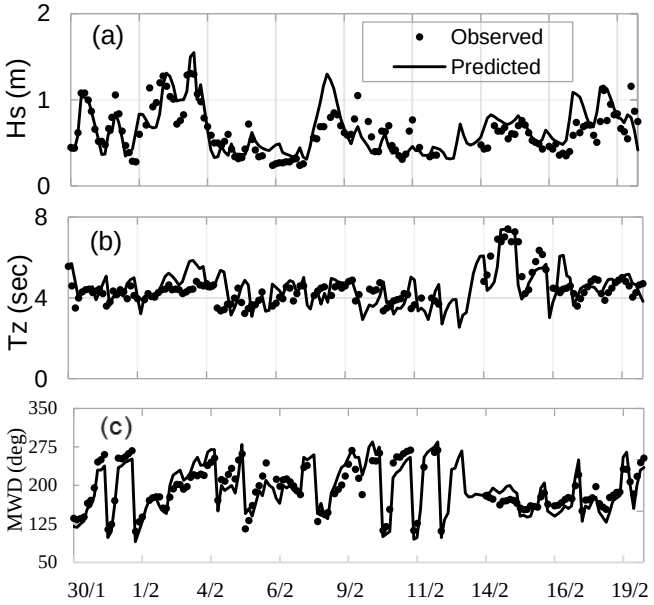

Figure 3. Time series plots of modeled and measured wave parameters at Chabahar buoy from Jan. 30, 2000 to Feb. 20, 2000: (a) significant wave height, (b) mean wave period, (c) mean wave direction

3.2.2. Kamphuis (1991)

Kamphuis (1991) also presented an equation based on dimensional analysis which is a function of combination of all the important terms influence on wave breaking and sediment movements:

$$Q = \frac{2.27 H_{sb}{}^2 T_p{}^{1.5} m_b{}^{0.75} D_{50}{}^{-0.25}\sin^{0.6}(2\alpha_b)}{(\rho_s-\rho_w)(1-n)} \qquad (3)$$

In which T_p= peak wave period, m_b= the beach slope in the surf zone and D_{50}= sediment median grain size.

3.2.3. Komar (1998)

Using breaker height and breaker angle, Komar (1998) proposed the following relationship:

$$Q = 0.46\rho_w g^{\frac{3}{2}} H_b{}^{\frac{5}{2}}\sin(\alpha_b)\cos(\alpha_b) \qquad (4)$$

For the present study, the aforementioned equations are compared with each other and validated against the net LST rate estimated based on the observed shoreline evolution pattern, dredging records and geomorphological features to determine the reliability of the figures of LST formulae for the study area.

4. Results

4.1. Wave Climate

The long-term variations in offshore wave climate were studied based on computing of mean annual wave data. Table 2 shows that mean annual significant wave height (H_s) varies from 0.27 m to 1.65 m with an average value of 0.82 m. The mean annual wave period (T_z) also varies between 3.6 sec and 12.3 sec, with an average magnitude of 6.85 sec. The coasts of Ramin are exposed to waves propagating annually from the sector

119° to 244°, with the average value of nearly 178° (Table 2).

Table 2. Long-term mean annual wave characteristics between 1985 and 2006

Wave parameters	Min.	Max.	Average	Standard deviation
Significant wave height (m)	0.27	1.65	0.82	0.09
Wave period (sec)	3.6	12.3	6.85	0.32
Mean wave direction (deg)	119	224	178.4	2.48

To assess the seasonal variations of the deep water wave climate for the region, monthly-based analysis of wave parameters was carried out. During the non-monsoon season, monthly average H_s ranges from 0.2 m to 1.13 m with the average of 0.48 m (nearly 95% of waves are with height less than 1 m) (Figure 4).

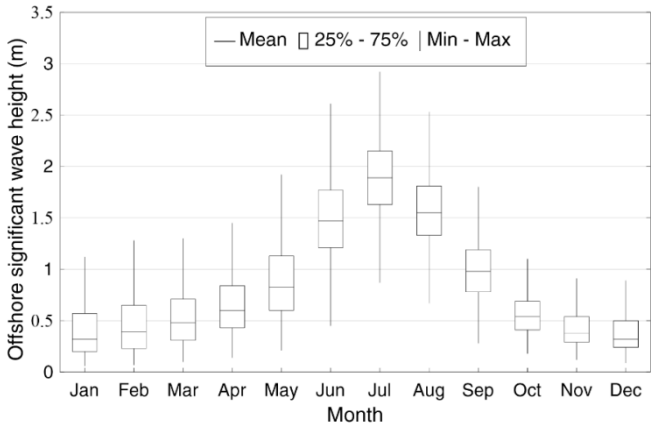

Figure 4. Monthly average of the offshore significant wave height for the 22 years of wave hindcast at WW3 hindcast node

End of pre-monsoon period is characterized by transition of low energy wind waves to high energy swell waves. Compare to other seasons, wave heights exhibit higher values during monsoon conditions and are observed within the range of 0.78 m to 2.15 m, with an average value of 1.5 m (88% of waves are greater than 1 m). Maximum H_s is experienced in July. The monthly average T_z during January to May varies from 4.2 sec to 8 sec. However, maximum T_z is observed in October and November (Figure 5).

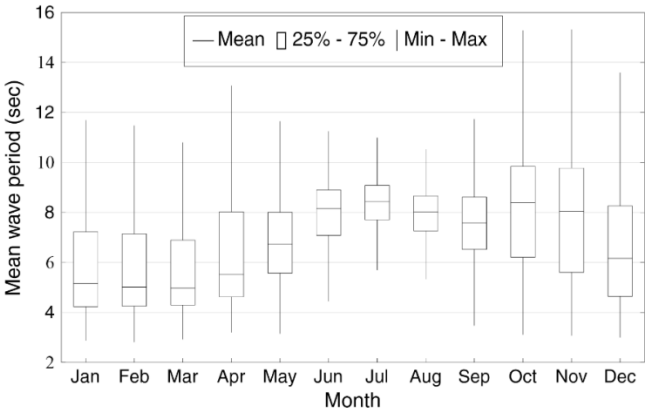

Figure 5. Monthly average of the mean wave period for the 22 years of wave hindcast at WW3 hincast node

The monsoon season is considerably less variable than the other seasons for the wave period and it mostly persisted between 6.5 sec and 9.1 sec with an average value of 8.05 sec. In addition, waves propagate over a very narrow directional band from the south section (Figure 6).

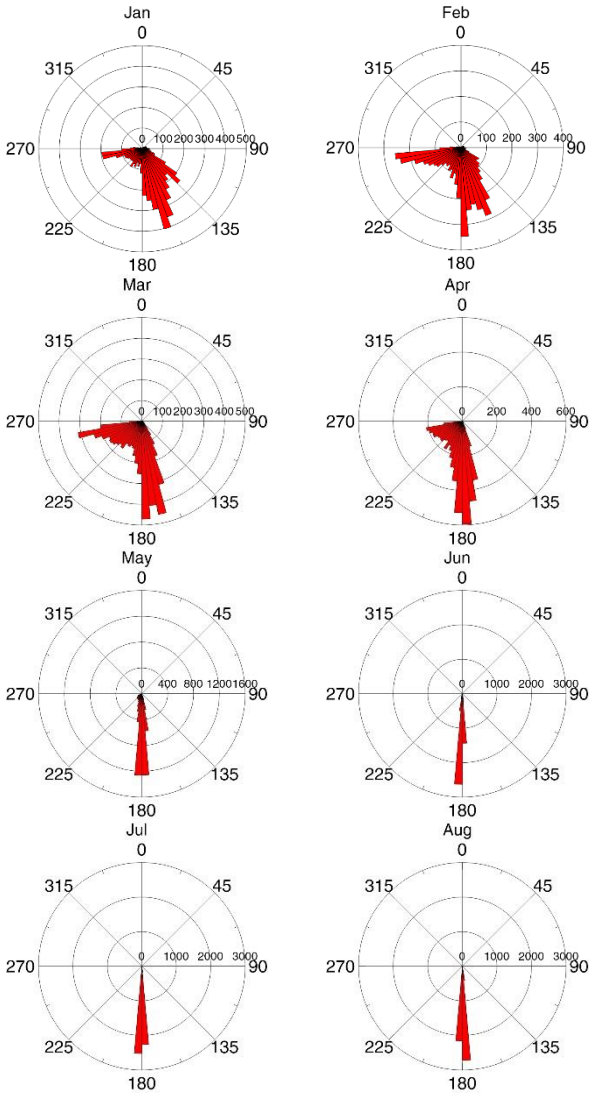

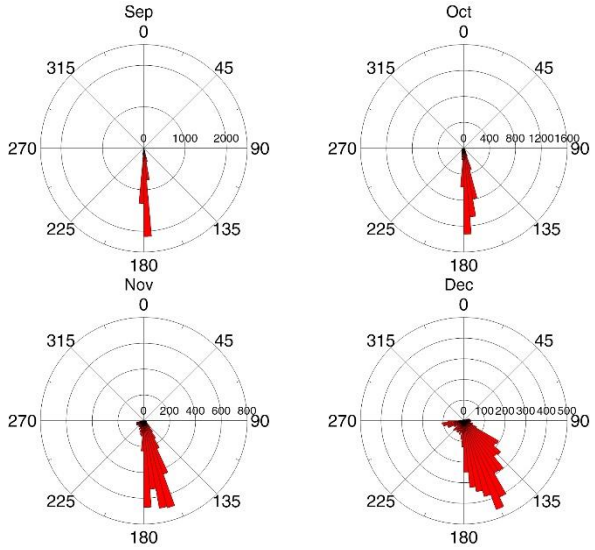

Figure 6. Rose diagram of monthly average of mean offshore wave direction for the 22 years of wave hindcast at WW3 hindcast node

About 10% of waves reach the coast from ESE to SSE, 70% of waves are between SSE and SSW and less than 20% of them approach from the sector between SSW and WSW. Further, with the onset of monsoon, long period swell waves propagating from south become predominant. Overall, the wave climate is dominated by high energy swell waves from south. However, significant seasonal variations in the wave conditions are experienced. The inter-annual variability of the deep-water wave parameters for the study site over a long period of 22 years, indicates that yearly wave characteristics are almost the same during the years (Figure 7). Furthermore, it presents an integration of clear annual cyclic pattern of monsoon waves and non-cyclic trend of non-monsoon waves.

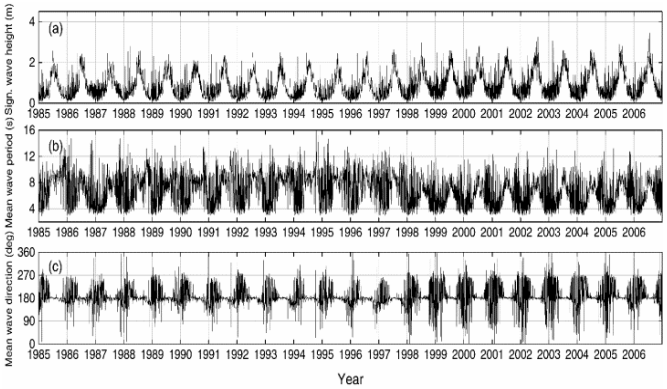

Figure 7. Inter-annual variability in wave parameters between 1985 and 2006: (a) significant wave height, (b) mean wave period, (c) mean wave direction

4.2. Longshore Sediment Transport Rate

Table 3 presents long-term mean annual net potential LST rates predicted by the selected methods for the study region. Comparative analysis of the long-term LST estimates obtained by different formulae indicates that the CERC equation overestimates the rate by about 136 and 39 percent than that of Kamphuis and Komar equation and the rate computed by the Komar formula is approximately 69 percent higher than Kamphuis equation. Mean annual net potential LST rates estimated with the CERC, Kamphuis and Komar expressions gave a value of 3.66, 1.55 and 2.63×10^5 m^3year^{-1} to the west, respectively.

Although the estimated magnitudes vary widely, all three formulae agree on the monthly and annual net LST direction. The variations of the net LST rate over a period of 22 consecutive years suggest that the annual net transport rates are quite variable from year to year (Figure 8). A roughly irregular pattern with a maximum value in 1996 and a minimum one in 2000 are observed during the examined period. The net LST direction was predominantly found towards the west. Reversals in the net transport directions occurred twice during the study period. The main reason for this phenomenon may be related to the very strong eastward transport as observed in 2000.

Table 3. Estimated long-term mean net potential LST rates

	CERC	Kamphuis	Komar
Potential LST ($10^5 m^3 year^{-1}$)	3.66	1.55	2.63

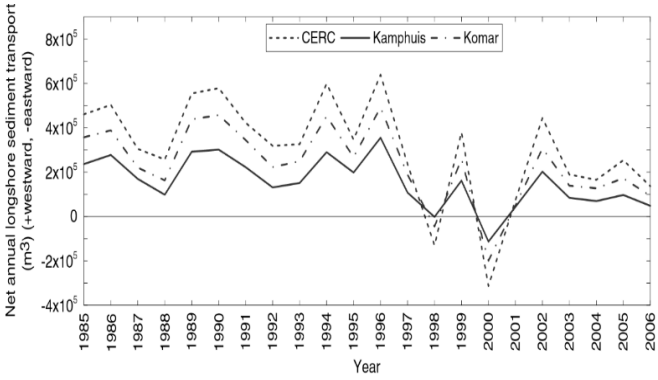

Figure 8. Annual estimations and inter-annual variability of the LST computed for the 22 years of wave hindcast based on the CERC (1984), the Kamphuis (1991) and the Komar (1998)

In order to provide the demonstration for the seasonal variability of LST, the net longshore transport was also examined based on monthly averages of 22-year (Figure 9). Seasonal variations in the LST rate are attributed to seasonal variations of the wave climate. Detailed analysis of the long-term monthly averages shows that the direction of net LST is from east to west throughout the year except during the monsoon months of June-July. As illustrated in Figure 6, the dominant direction of the wave is from SSE to S during the year, causing a large amount of sediment transport in westerly direction. It was also found that the wave height describes low energy conditions during the non-monsoon season, while during the monsoon season the wave energy increases and the waves are consistently high, which has a direct effect on the transport rate.

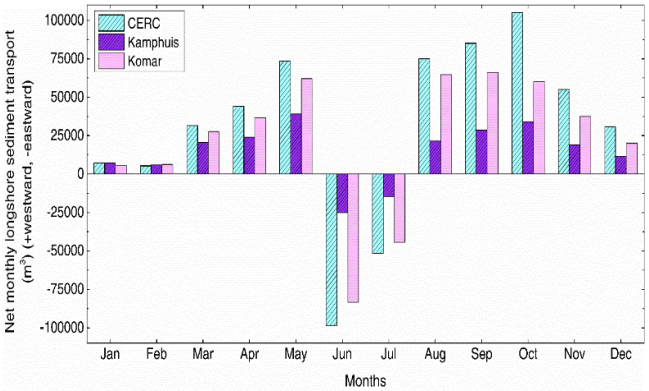

Figure 9. Monthly average net LST rate estimated at the breaker zone for the 22 years of wave hindcast from the CERC (1984), the Kamphuis (1991) and the Komar (1998)

H_s within the monsoon period was 3 times the value during non-monsoon period. The computed LST rate based on the CERC, Komar and Kamphuis during monsoon period (4 months) was 54, 50 and 36 %, respectively, of the total LST rate. The non-monsoon season (8 months) contributes to about 46, 50 and 64 % based on the same formulae.

The performance of the LST rates calculated from the CERC formula noticeably depend on the values considered for the *K* empirical coefficient.Various values of the *K* coefficient have been presented by the researchers over the last decades (e.g., Bailard, 1981, 1984; Kamphuis and Readshaw, 1978; del Valle, Medina, and Losada, 1993). However, the default value for this parameter recommended by Komar and Inman (1970) employed in this study yielded unsatisfactory results. Then, the Komar formula produced the estimation close to that calculated by the CERC formula since both the formulae have the same input parameters that need to be calibrated and adjusted with the field data. The Kamphuis expression gives values significantly smaller than the values obtained by the CERC and Komar.

5. Discussion

The magnitudes of potential LST calculated using the hindcast wave data and empirical formulae may overestimate or underestimate the transport rates under different conditions and at different sites. In addition, the above LST relationships suffer from uncertainties arising from local conditions in which they were developed and are also based on the assumption of infinite supply of sand along the shoreline. In order to achieve logical long-term net longshore transport rates, a number of verifications are usually required for the geomorphology of the study area. Coastal landforms respond to all the variables of shore drift during their course of formation and hence these landforms can be considered the most reliable of long-term sediment transport indicators (Kunte and Wagle, 1993). The coastline between the Chabahar Bay and Ramin Harbor is dominated by rocky coral beaches to the west, near the Chabahar Bay. Further east, until Ramin Harbor, it consists of sandy beaches, which are limited landward by cliffs. The coast between Ramin Harbor and Beris Headland is partially rocky, along with straight sandy beaches backed by coastal dune systems. Sand bar formed at the mouth of Lipar seasonal river on the updrift (east) side of the Ramin Harbor blocks sediment load discharge to the sea (Figure 10). Hence, the Ramin Harbor is situated in a supply limited coast.

Figure 10. Geomorphic landforms along the coastline extent between Chabahar Bay and Beris Headland

The sediment transport regime can also be inferred from the established shoreline movement trend across the study area. A relative stability in shoreline position can be found both on up-drift and down-drift sides of the harbor, while an accretion trend may be detected at the beach leaned to the secondary breakwater (Figure 11). Dredging operations performed in 2004 are responsible for the considerable shoreline retreat within the outer basin of the harbor.

Numerical simulations conducted by Isaie Moghaddam et al. (2018), indicate that coastal currents over the study area flow toward the outer port basin and form

cyclonic gyres that contribute in transporting and depositing coastal sediments within the port basins and around the secondary breakwater. These corroborates that the net LST direction is westbound (into the harbor basins). In other words, the outer harbor basin acts as the substantial sediment sink which entrapped the majority of littoral sand coming from east coast of Ramin. Therefore, the real (or actual) net LST rate can be equated to the amount of sediments accumulated in harbor basins.

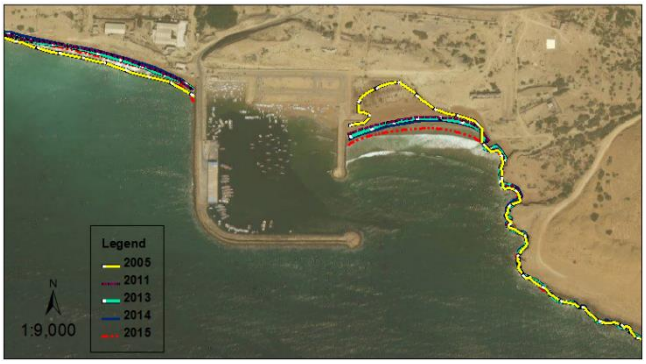

Figure 11. Historical shoreline position at the study area over a 10-year period (instantaneous wet/dry line proxy)

Also, in order to determine actual net LST rate across the study area, volumetric differences based on hydrographic surveys and dredging records may be used. Two bathymetric surveys carried out in 2000 and 2009 at the nearshore zone of the Ramin Harbor. However, the survey interval is not short enough to identify different seasonal changes. Concern to dredging activities, the regions adjacent to the harbor mouth and the secondary breakwater, where the majority of sediments are deposited were frequently dredged. The amounts of materials removed in 2002 and 2004 were about 0.625×10^5 m^3 and $0.658\times10^5 m^3$, respectively. These dredging figures yield the associated actual net LST rate about 0.3×10^5 $m^3 year^{-1}$ at Ramin Harbor.

Evaluation of coastal landforms, geomorphological indicators and dredging records of the coastal stretch under consideration suggest that the availability of sand at the littoral section has been restricted. Then, it may be concluded that actual longshore transport rate will be significantly less than that of the calculated potential rate. Moreover, the magnitudes of potential LST calculated based on CERC and Komar formulae overestimated the transport rates and can lead to large coastline variations which were not observed along the study area. However, the rates estimated based on the Kamphuis expression are considered more suitable for the evaluation area. This confirms the results of Afshar-Kaveh and Soltanpour (2010), who suggested the Kamphuis (1991) equation as offering reliable formula along the Iranian southern coasts. Moreover, Schoonees and Theron (1996) and Schoonees (2001), evaluated the efficiency of 52 different LST formulae against an extensive database collected at a wide variety of sites around the globe and found that the Kamphuis (1991) formula is the most accurate overall (Schoonees, Theron, and Bevis, 2006).

6. Conclusions

Estimates of the annual and inter annual LST variations along the Ramin Harbor, southeast coastline of Iran, have been determined using 22 years hindcasted wave data. Annual cycle of wave climate over the study area was dominated by two distinct seasonal changes: high energy waves from southern sector with an average period of 8.05 sec and height range from 0.78 to 2.15 m during monsoon season, and long period swells spreading from southeast to south direction superimposed with variable wind waves from west to southwest with the average period of 6.25 sec and wave height of 0.48 m during non-monsoon period. Computed long-term mean net potential LST rate for the region is 3.66, 1.55 and $2.63\times10^5 m^3 year^{-1}$ based on the CERC, Kamphuis and Komar formulae, respectively. The seasonal variation in LST rate was also observed in response to the seasonality of wave regime. Multiple lines of evidences have been deployed to evaluate the predicted LST magnitudes and directions. For this case study, the investigation was made at sandy beaches bounded with short stretches of rocky outcrops, where geologic features normally control sediment transport. Consequently, the actual longshore transport rate was less than the potential transport rate. It has then been found that the Kamphuis formula yielded more acceptable values in comparison with the other two formulae. In addition, a net sediment transport to the west was inferred from calculations and environmental observations.

Acknowledgments

Authors acknowledge Iranian Ports and Maritime Organization (PMO) and Iranian National Institute for Oceanography and Atmospheric Science (INIOAS) for making the wind and wave data available. The first author also wishes to express his sincere thanks to Kh. Bahiraie for his keen interest and encouragement, and also to Dr. A. Nasrollahi for his valuable explanations of MIKE software applications and suggestions which greatly improved quality of this research study. This work would not have been possible without availability of the MIKE 21 product provided by Danish Hydraulic Institute (DHI) and their contribution is greatly appreciated.

References

1- Afshar-Kaveh, N. and Soltanpour, M., (2010), *Verification of longshore sediment transport formulas at some of the southern coastlines of Iran*, Journal of

Civil and surveying Engineering, Vol.44(3), p.317-326.

2- Bailard, J. A., (1981), *An energetics total load sediment transport model for a plane sloping beach*, Journal of Geophysical Research, Vol. 86.

3- Bailard, J. A., (1984), *A simplified model for longshore sediment transport*, Proceedings of the 19th International Conference on Coastal Engineering, p.1454-1470, Houston, Texas.

4- Battjes, J. A. and Janssen, J. P. F. M., (1978), *Energy loss and set-up due to breaking of random waves*, Proceedings of the 16th International Conference on Coastal Engineering, p. 569-587, Hamburg, Germany.

5- Camenen, B. and Larroudé, P., (2003), *Comparison of sediment transport formulae for the coastal environment*, Coastal Engineering, Vol.48(2), p.111-132.

6- CERC, (1984), *Shore protection manual*. Washington: Coastal Engineering Research Center, U.S. Army Corps of Engineers Press.

7- Chempalayil, S. P., Kumar, V. S. and Dora, G. U. and Johnson, G., (2014), *Near shore waves, long-shore currents and sediment transport along micro-tidal beaches, central west coast of India*, International Journal of Sediment Research, Vol.29(3), p.402-413.

8- del Valle, R., Medina, R. and Losada, M. A., (1993*), Dependence of coefficient K on grain size*, Journal of Waterway, Port, Coastal and Ocean Engineering, Vol.119(5), p.568-574.

9- *DHI MIKE 21 Wave modeling user guide*, (2014), Denmark: DHI Water and Environment.

10- Dibajnia, M., Kebriaee, A., and Allahyar, M., (2008), *Wave climate hindcast for the Oman Sea*, Proceedings of the 8th International Conference on Coasts, Ports and Marine Structures p.29-31, Tehran, Iran.

11- Güner, H. A. A., Yüksel, Y. and Çevik, E. Ö., (2013), *Longshore sediment transport-field data and estimations using neural networks, numerical model, and empirical models*, Journal of Coastal Research, Vol.29(2), p.311-324.

12- Isaie Moghaddam, E., Hakimzadeh, H., Allahdadi, M.N., Hamedi, A., Nasrollahi, A., (2018), *Wave-induced currents in the northern Gulf of Oman: a numerical study for Ramin Port along the Iranian coast*, American Journal of Fluid Dynamics, Vol.8(1), p.30–39.

13- Kamphuis, J. W., (1991), *Alongshore sediment transport rate*, Journal of Waterway, Port,

14- Coastal and Ocean Engineering, Vol.117(6), p.624-640.

15- Kamphuis, J. W. and Readshaw, J. S., (1978), *A model study of alongshore sediment transport rate*, Proceedings of the 16th International Conference on Coastal Engineering, p.1656-1674, Hamburg, Germany.

16- King, D. B. Jr., (2005), *Influence of grain size on sediment transport rates with emphasis on the total longshore rate (Technical report of ERDC/CHL CHETN-II-48)*, Washington: U.S. of Army Corps of Engineers.

17- Komar, P. D., (1998), *Beach processes and sedimentation*, p.544-545, New Jersey: Prentice Hall Inc. Press.

18- Komar, P. D. and Inman, D. L., (1970), *Longshore sand transport on beaches*, Journal of Geophysical Research, Vol.75(30), p.5914-5927.

19- Kunte, P. D. and Wagle, B. G., (1993), *Remote sensing approach to determine net shore drift direction-a case study along the central east coast of India*, Journal of Coastal Research, Vol. 9(3), p.663-672.

20- Larangeiro, S. H. C. D. and Oliveira, F. S. B. F., (2003*), Assessment of the longshore sediment transport at Buarcos beach (west coast of Portugal) through different formulations*, In Proceedings of CoastGIS'03, Genova, Italy.

21- Mafi, S., Yeganeh-Bakhtiary, A. and Kazeminezhad, M. H., (2013), *Prediction formula for longshore sediment transport rate with M5' algorithm*, Journal of Coastal Research, Vol.2(SI 65), p.2149-2154.

22- Prasad, K. and Reddy, B., (1988), *Near-shore sediment dynamics around Madras Port, India*, Journal of Waterway, Port, Coastal and Ocean Engineering, Vol.114(2), p.206-219.

23- Schoonees, J. S., (2000), *Annual variation in the net longshore sediment transport rate*, Coastal Engineering, Vol.40(2), p.141-160.

24- Schoonees, J. S., (2001), *Longshore sediment transport: applied wave power approach, field data analysis and evaluation of the formulae*, PhD thesis, University of Stellenbosch, Stellenbosch.

25- Schoonees, J. S. and Theron, A. K., (1996), *Improvement of the most accurate longshore transport formula*, Proceedings of the 25th International Conference on Coastal Engineering, Vol.3, p.3652-3665, Orlando, Florida.

26- Schoonees, J. S., Theron, A. K. and Bevis, D., (2006), *Shoreline accretion and sand transport at groynes inside the Port of Richards Bay*, Coastal Engineering, Vol.53(12), p.1045-1058.

27- Shanas, P. R. and Sanil Kumar, V., (2014), *Coastal processes and longshore sediment transport along Kundapura coast, central west coast of India*, Geomorphology, Vol.214, p.436-451.

28- Sheela Nair, L., Sundar, V. and Kurian, N. P., (2015), *Longshore sediment transport along the coast of Kerala in southwest India*, Proceedings of the 8th International Conference on Asian and Pacific Coasts, Vol.116, p.40-46, Chennai, India.

29- Short, A. D., (1991), *Macro-meso tidal beach morphodynamics-an overview*, Journal of Coastal Research, Vol.7(2), p.417-436.

30- Short, A. D. and Hesp, P. A., (1982), *Wave, beach and dune interactions in southeastern Australia*, Marine Geology, Vol.48(3-4), p.259-284.

31- Smith, E. R., Wang, P., Ebersole, B. A. and Zhang, J., (2009), *Dependence of total longshore sediment transport rates on incident wave parameters and breaker type*, Journal of Coastal Research, Vol.25(3), p.675-683.

32- Tolman, H. L., (2009), *User manual and system documentation of WAVEWATCH III version 3.14 (Technical Note 276)*, National Oceanic and Atmospheric Administration (NOAA), Camp Springs, MD 20746.

33- Walters, K. R. and Sjoberg, W. F., (1988), *The Persian Gulf region, a climatological study*, Washington: U.S. Marine Corps, Department of the Navy Press.